Energy dependence of the outer core-level multiplet structures in atomic Mn and Mn-containing compounds

B. D. Hermsmeier,* C. S. Fadley,† and B. Sinkovic‡
Department of Chemistry, University of Hawaii, Honolulu, Hawaii 96822

M. O. Krause, J. Jimenez-Mier,§ P. Gerard,‖ and T. A. Carlson
Oak Ridge National Laboratory, Oak Ridge, Tennessee 37831

S. T. Manson and S. K. Bhattacharya
Department of Physics and Astronomy, Georgia State University, Atlanta, Georgia 30303
(Received 17 March 1993)

We consider the energy dependence of the Mn 3*s* and 3*p* multiplets from gas-phase atomic Mn and crystalline MnF_2 and $KMnF_3$ over the range from x-ray photoelectron spectroscopy (XPS) energies down to energies near threshold. First comparing atomic and solid-state spectra for these multiplets permits concluding that the splittings in the compounds MnF_2, MnO, and $Cd_{0.3}Mn_{0.7}Te$ are highly atomic in character, with no significant effects due to extra-atomic screening. Measuring the energy dependence for atomic Mn, MnF_2, and $KMnF_3$ then shows for both the 3*s* and 3*p* multiplets that there is a decrease in the intensities of the higher-binding-energy quintet states relative to those of the corresponding septet states as the excitation energy is lowered. This effect on the quintet:septet branching ratios is also found to extend to rather high energies, with the ratios at the XPS limit of $\approx$1400 eV above threshold being approximately 25–30% greater than those at $\approx$200 eV above threshold. We show that this energy-dependent final-state branching ratio is not due simply to spin-dependent dipole matrix elements as derived from single-configuration Hartree-Fock calculations. We suggest that this effect is caused by the sudden-to-adiabatic transition, which at lower energies favors the exchange-stabilized septet states that are the ground states of the ions formed. However, two prior theoretical models for such sudden-to-adiabatic intensity changes [Stohr, Jaeger, and Rehr, Phys. Rev. Lett. **51**, 821 (1983) and Thomas, Phys. Rev. Lett. **54**, 182 (1985)] were not found to describe our results well, particularly in the extension of the effect to higher energies. We consider qualitatively a configuration-interaction model with quintet-septet interchannel coupling that may better describe these effects and form the basis for more quantitative calculations.

INTRODUCTION

Attempts to acquire a clear understanding of photoionization processes in the near-threshold energy region have attracted considerable attention during the past several decades. Many-body and relativistic effects inherent in the physics of these processes make many aspects of these phenomena very difficult to treat at levels of sufficient exactness, but there is nonetheless a considerable literature dealing with the energy dependence of such phenomena as shakeup and shakeoff.[1–19] In this paper, we consider the detailed behavior of the relative intensities of Mn 3*s* and Mn 3*p* outer-core multiplet features as threshold is approached. Several aspects of the behavior of these relative intensities will be found to suggest a connection to the sudden-to-adiabatic transition as excitation energy is decreased. We thus begin by briefly reviewing some key prior studies which have attempted to explain the near-threshold energy-dependent responses for final-state phenomena such as core-level shakeup or shakeoff satellites and outer-core-level multiplet splittings. We then consider briefly what is known about the positions and relative intensities of the Mn 3*s* and Mn 3*p* multiplets for high excitation energies that can be considered to be in the sudden limit. We then discuss new experimental results for the energy dependence of outer-core-level multiplets from Mn^{2+}-containing compounds and gas-phase atomic Mn.

As a prelude to the discussion of the energy dependence of shakeup, shakeoff, and multiplet processes, we first discuss some of their fundamental similarities. Because we are dealing with photoionization, all final states must be reached by a dipole photoabsorption process which at the low energies considered here is an excellent approximation.[1–3] The wave functions necessary for describing many shakeup and shakeoff processes, as well as certain multiplet processes, must be more accurate than a single-configuration Hartree-Fock (HF) approach. The most common method for generating more accurate wave functions is that of configuration-interaction (CI), and Manson[2] has discussed the use of such wave functions for calculating photoexcitation cross sections (σ) by systematically varying the number of configurations in the initial- and final-state wave functions employed. The dominant configuration in the initial state is the HF configuration, with usually slight perturbations to allow for correlation effects coming from other configurations

with smaller mixing coefficients. However, the final state of the isolated ion contains a core hole which significantly alters the orbitals of the remaining electrons via relaxation. To treat the photoemission process correctly, we must in addition take into account that the final state contains both a continuum photoelectron state and a core hole. At higher energies, there is little coupling between the ion and the photoelectron, and thus the calculation of the ionic wave functions and the continuum orbitals can be separated in evaluating σ; this leads to the well-known sudden approximation (SA) limit that has been used to describe many types of fine structure in photoelectron spectra[1-23] and can be used to evaluate the final-state ionic wave functions. But in the near-threshold energy regime, the photoelectron-ion coupling becomes stronger and the adiabatic limit is ultimately reached.

A. Shakeup and shakeoff in atoms

Historically, the first experimental studies attempting to probe the question of near-threshold energy dependence of satellite lines involved noble gases such as Ne (Refs. 4 and 5) and Ar (Ref. 6). In these and later[7,8] investigations, the goal was to identify and assign the satellites associated with the main spectral features and to describe their behavior in the threshold region. In the high-energy limit, the satellite intensities relative to the main lines could be explained in a satisfactory manner using the sudden approximation. In this picture, an effective positive charge suddenly appears, thus "shaking" the other electrons in the system, and leading to an excitation or further ionization of the ion. With the previously mentioned separation of photoelectron and shakeup or shakeoff excitations, the latter are found to follow monopole selection rules in which the probability for such an excitation is given by the overlap of the initial- and final-state wave functions for the $(N-1)$ electrons of the ion. However, for energies near threshold for which the electron leaves the vicinity of the ion slowly and can thus be influenced by the various ionic relaxation or even decay processes, the interaction of the photoelectron with the ion, including, perhaps, *interchannel coupling* effects must be considered. For such energy dependence to be calculated in fullest generality, the final-state N-electron wave function must include configurations representing all optically allowed final N-electron states, whether this is by direct photoexcitation or some other process (e.g., autoionization). We will later suggest that interchannel coupling may be needed to describe the energy dependence of multiplet intensities seen in our study.

There have been numerous experimental and theoretical studies of atomic shakeup and shakeoff phenomena, but controversy still persists over the interpretation of some of these results.[4-15] Even in the high-energy limit where interchannel coupling can be neglected, CI calculations,[9,10] as discussed in Ref. 11, were not able to accurately predict relative intensities of the Ar $3s^{-1}$ photoelectron spectrum. One trend that is common to most atomic studies and is particularly relevant to the topic of this study centers on the gradual decrease in the shakeup or shakeoff satellite intensities as threshold is approached from the high-energy limit. Although exceptions to this trend do exist due to specific many-electron interactions and resonances, we will in the following concentrate on the simpler and limiting behavior of the majority of cases studied to date.

This variation of shakeup and shakeoff satellite intensity with energy has been considered quantitatively by Stohr, Jaeger, and Rehr[16] and by Thomas.[17] These authors have used two rather different models which qualitatively agree in some respects, but predict very different functional forms for the variation of satellite intensity as energy is increased from threshold. Both models predict a rapid convergence to the sudden limit that is also more rapid as the energy separation (ΔE) between the main line and a given satellite structure becomes smaller. And conversely, the greater the splitting, the more gradual will be the adiabatic-to-sudden convergence for a given system. However, the model of Stohr, Jaeger, and Rehr[16] does not include time explicitly, but considers the photoelectron-ion coupling for a given shakeup state to involve an interference between "direct" and exchange" excitations to reach a given final state. The two excitations are: direct—core-to-photoelectron by dipole excitation plus valence (a) to valence (b') by monopole excitation and exchange—core-to-valence (b') by dipole plus valence (a) to photoelectron by monopole. With some assumptions concerning relative matrix elements that have subsequently been questioned by Thomas,[17] they arrive at an expression for the satellite relative intensity or branching ratio (R) at a given photoelectron kinetic energy ($E_{\rm kin}$) above threshold of the form

$$R = R_{\rm SA}|1-(\Delta E/E_{\rm kin})^2|^2 , \tag{1}$$

where $R_{\rm SA}$ is the branching ratio in the sudden approximation limit, usually measured in practice with typical x-ray photoelectron spectroscopy (XPS) excitation. Time is thus implicitly included in the sense that the photoelectron energy influences the relevant matrix elements and overlaps involved. A more accurate treatment of the same sort of direct-plus-exchange model has been considered subsequently by Armen *et al.*[8] in connection with Ar $1s$ shakeup in Auger excitation; they include all relevant matrix elements and overlaps, but this does not yield a simple expression such as Eq. (1) that can be applied to other cases easily.

Thomas[17] by contrast, has used a time-dependent approach that is very similar to that applied by Gadzuk and Sunjic[18] to the analysis of line shapes in core emission from metals. This involves determining the time that is required for the photoelectron to leave the system by dividing a characteristic dimension of the system (d) by its classical velocity at energy $E_{\rm kin}$. The final expression for R in this case is

$$R = R_{\rm SA}\exp(-md^2\Delta E^2/2h^2E_{\rm kin}) , \tag{2}$$

$$= R_{\rm SA}\exp(-d^2\Delta E^2/15.32E_{\rm kin}) , \tag{3}$$

where m is the mass of the electron, d is in Å, and energies are in eV. This model is found by Thomas[17] to agree reasonably well with neon shakeoff intensities as measured by Carlson and Krause.[4] We comment further on the agreement of both of these models with specific experimental data below.

As noted above, Armen *et al.*[8] have attempted to understand the energy dependence of Ar 1*s* shakeup or shakeoff features on approaching threshold by measuring the satellites associated with the $KL_{2,3}L_{2,3}$ Auger lines. The threshold for excitation is the Ar 1*s* binding energy of approximately 3206 eV. Their shakeup satellite intensity showed very little energy dependence over the photon energy range of 5200–3250 eV, followed by an abrupt intensity drop in the 3240–3220 eV range, or only 14–34 eV above threshold. For the shakeoff satellite, the decrease in intensity was found to be much more gradual, beginning at higher photon energies of $\approx$3350 eV, or 150 eV above threshold. Thus, its behavior is notably different from the shakeup peak. Armen *et al.*[8] and Dyall[19] have made quantitative predictions for the energy dependence of both of these Ar satellites based on single-configuration HF and full-CI calculations, respectively. As noted before, the calculations of Armen *et al.* include both direct and exchange terms, but in a more accurate way than the model leading to Eq. (1). The energy dependence of the shakeup intensities is poorly predicted by both calculations at energies within approximately 35 eV of threshold. In contrast to this poor agreement for the shakeup data, the agreement in the shakeoff data was much better for both the gradual decrease of the shakeoff intensity as the photon energy ($h\nu$) is decreased near threshold and the flatness of the curve in the higher-energy regime.[8,10] Overall, these results are at least qualitatively consistent with both Eqs. (1) and (2) in showing a more gradual approach to the sudden limit for the shakeoff effects in 1*s* excitation that are at a higher energy from the main line. As expected, the use of Auger satellites to monitor core-excitation shakeup and shakeoff yields decreases in intensities for excited states on approaching threshold that are very similar to the effects observed in core photoelectron spectra.

B. Multiplet-split levels

We now consider the case of most direct relevance to this paper: the energy dependence of outer-core-level multiplets in high-spin transition-metal atoms and solids. These multiplets are well known and arise when a core hole interacts with a partly filled valence electron shell.[1,20] This interaction was first interpreted in terms of a strongly intra-atomic *L-S* term splitting in the final state with the hole present. For the simplest case of emission from an *ns* level in a 3*d* atom, the *L-S* picture predicts a doublet with a separation proportional to $(2S+1)K(ns\text{-}3d)$, where S is the initial spin of the partially filled 3*d* subshell and $K(ns\text{-}3d)$ is the *ns*-3*d* exchange integral. It is the branching ratio of the resulting doublet with which we will be concerned; this corresponds to $S-1/2$ and $S+1/2$ final states.

For the case of principal experimental interest here, Mn 3*s* emission from atomic Mn or Mn^{2+} in a ^6S initial state with $S=\frac{5}{2}$, a simple estimate of the splitting between ^5S and ^7S using the 3*s*-3*d* exchange integral gives an energy splitting of about 13 eV that is approximately a factor of 2 greater than the experimental value of 6.5 eV found in compounds containing Mn^{2+}. It has been thought for some time that the basic origin of the reduced splitting is due to an enhanced degree of electron-electron correlation in the low-spin final state that is not properly included in a HF calculation. This conclusion is based on atomic calculations including CI by Bagus, Freeman, and Sasaki.[21] An alternative viewpoint has more recently been expressed by Veal and Paulikas, who have emphasized extra-atomic screening phenomena together with multiplet splittings.[22(a)] But both older experimental studies on Mn compounds by Kowalczyk *et al.*[23] and more recent work on both atomic Mn and other Mn compounds by Hermsmeier *et al.*,[24] provide very strong support for the idea of highly intra-atomic multiplet splittings modified by spin-specific correlation effects, as embodied in the ideas of Bagus *et al.*[21]

We consider this controversy in some more detail because it serves to introduce some essential aspects of the spectra whose branching ratios we will study. In describing 3*s* multiplet splittings for several transition-metal compounds, Veal and Paulikas[22(a)] argued for a strong involvement of extra-atomic screening processes similar to those considered in the case of N_2 on Ni(110).[16] Thus, they suppose "screened" and "unscreened" manifolds of states within which multiplet splittings occur. The screened manifold is further assumed to be associated with extra-atomic charge transfer of a full screening electron into a bound Mn 3*d* orbital and/or more diffuse Mn 4*s*/4*p* orbitals. Empirical parameters for separation and relative intensity of screened and unscreened peaks were derived from deeper-level 2*p* core spectra, and the relative intensities within the two multiplets were corrected by making use of the CI results of Bagus *et al.*[21] Although they obtain rather good agreement with experiment for a series of compounds, their assumptions are not fully self-consistent.[24] The experimental evidence that provides proof of the highly intra-atomic nature of these particular splittings and the error of this model is shown in Fig. 1. Here, we compare the Mn 3*s* multiplet manifolds for four distinct cases: atomic Mn(*g*), MnF_2(*s*), MnO(*s*), and $Cd_{0.3}Mn_{0.7}Te$(*s*), with the three solids being listed in order of increasing covalency. It is immediately obvious that the dominant doublet, i.e., the peaks labeled ^7S and $^5S(1)$, in all three solids has essentially the same splitting as that of the atomic multiplet. It is also striking that even the two weaker peaks labeled as $^5S(2)$ and $^5S(3)$ are essentially identical for Mn, MnF_2, and MnO. This strong similarity between atomic and solid-state spectra thus suggests a common origin for the splittings and weaker satellites. The Mn atom with its high-spin $[3d^5 4s^2]$ configuration can neither make use of extra-atomic relaxation (as it is not bound to anything) nor rearrange itself as a pseudoscreened $[3d^6 4s^1]$ configuration with the correct total final state required.[24] Thus it is impossible for this case to include any sort of equivalent of the extra-atomic charge transfer considered by Veal and Paulikas, and their model must be ruled out for these cases and probably also others for which the ionicity is sufficiently high. In a very recent paper by Oh, Gweon, and Park,[22(b)] the effects of exchange splittings, intrashell electron correlation, and final-state hole screening have been considered in a more rigorous theoretical

model and compared with a more extensive set of solid-state experimental data for compounds of varying ionicity. This work agrees with our conclusions for highly ionic systems, but goes on to point out that the degree to which screening may distort the simple multiplet interpretation increases with increasing covalency.

The results in Fig. 1 can also be compared with theory, for which the vertical bars in Fig. 1(e) are taken from the CI calculations of Bagus *et al.*[21] The several ^5S states [labeled arbitrarily $^5S(1)$, $^5S(2)$, and $^5S(3)$] are the result of final-state configuration interaction between $3s^1 3p^6 3d^5$ and $3s^2 3p^4 3d^6$. The $^5S(1)$ state nearest ^7S has the largest admixture of the $3s^1 3p^6 3d^5(^6S)$ configuration. These theoretical predictions are also in excellent agreement with experimental results for both the free atom and solid-state ionic compounds, leaving little doubt as to the correct approach for describing this process in the sudden limit.

In analogy with the shakeup, shakeoff, and screening features already discussed, multiplets are also final-state effects for which the features at lower photoelectron kinetic energies are associated with more highly excited ionic states. Thus, they too might be expected to exhibit an intensity decrease as the excitation energy is decreased to a more adiabatic region near threshold. In studying whatever sudden-to-adiabatic effects may be present, it is important to avoid such many-electron complications as resonant photoemission and interference by Auger transitions. With these processes excluded, it would thus be expected for Mn^0 or Mn^{2+} that the $ns \rightarrow \epsilon p$ emission process should yield only the ^7S state in the adiabatic limit. We will explore how this limit is approached and begin by considering briefly some prior work on outer-shell emission to provide some guidance.

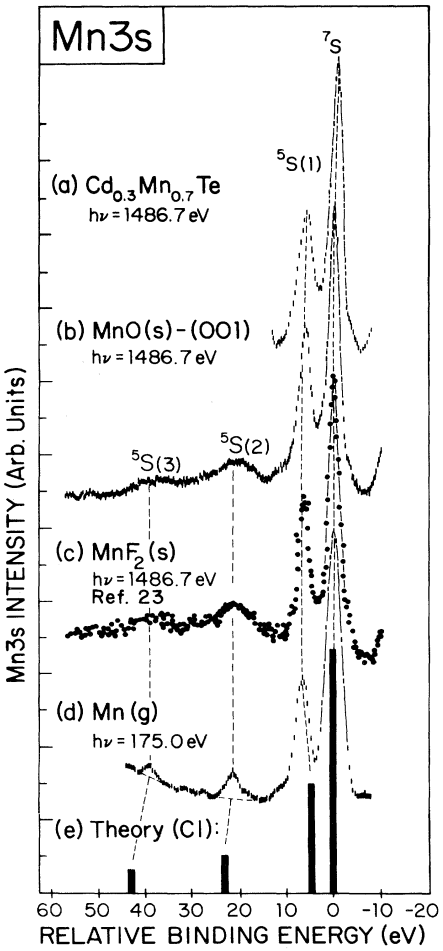

FIG. 1. Experimental Mn 3*s* spectra for (a) single-crystal $Cd_{0.3}Mn_{0.7}Te$, (b) MnO(001), (c) polycrystalline MnF_2 (Ref. 36), and (d) gas-phase atomic Mn are compared to (e) theoretical calculations for emission from a free Mn^{2+} ion including configuration interaction (CI) effects (Ref. 21).

The first experimental energy-dependent studies on a multiplet of Mn^0 were reported by Bruhn *et al.*[25] and Krause, Carlson, and Fahlman[26] who monitored the Mn 4*s* photoelectron region. Krause, Carlson, and Fahlman[26] plotted the 4*s* branching ratio over the energy range 16 to 56 eV and found two points of interest: first, the branching ratio (^7S:^5S) had a distinct dip in the $3p \rightarrow 3d$ resonance region and second, as the photon energy was decreased further, the intensity of the ^5S began to decrease relative to the ^7S intensity. But at photon energies of approximately 17 eV, i.e., about 10 eV above the 4*s* threshold, the branching ratio went through large oscillations. A plausible explanation for such behavior was 4*s* coupling with the $3d \rightarrow nl$ Rydberg states. Thus, although there are other effects which appear to complicate the 4*s* branching ratio over this energy range, an indication remains that the relative intensity of the ^5S state decreases relative to the ^7S configuration near threshold. This is thus consistent with, but not conclusive of, a linkage to a continuous breakdown of the sudden approximation as threshold is approached.

We now turn to a much better candidate for this study: Mn 3*s* emission. Unlike Mn 4*s*, which must pass through various 3*p* and 3*d* resonance states when approaching threshold, the 3*s* is a core level with a binding energy of approximately 100 eV (see Table I). Thus, the relevant photon energies are all well above the excitation thresholds for these resonances. Since 3*s* shares the same principal quantum number as 3*d*, their overlap will be the largest and therefore display the greatest degree of splitting.

TABLE I. Manganese 3*s* and 3*p* multiplet binding energies (E_b) and energy separations (ΔE).

Ionic state	E_b (eV)	ΔE (eV)
$3s$: ^7S	92.8	0
$^5S(1)$	99.3	6.5
$^5S(2)$	113.7	20.9
$^5S(3)$	132.0	39.2
$3p$: ^7P	57.3	0
$^5P(1)$	60.4	3.1
$^5P(2)$	63.9	6.6
$^5P(3)$	67.8	10.5
$^5P(4)$	75.0	17.7

We have thus studied the energy dependence of Mn 3*s* emission from both solid Mn compounds containing high-spin Mn^{2+} and atomic Mn. In the following sections we present these new data, considering first the energy dependence found in the branching ratio $^5S:^7S$ of the Mn 3*s* multiplet. We also consider data for two 3*p* multiplet branching ratios, and show that it exhibits very similar behavior, even though its origins are more complex and hence less certain. The solid-state data were obtained from two rather ionic Mn^{2+} compounds, single-crystal $KMnF_3$ (110) and polycrystalline MnF_2, over the excitation energy range 200–1500 eV. Some results for the more covalent but still high-spin $Cd_{0.3}Mn_{0.7}Te$(111) are also presented. The gas-phase data were obtained from monatomic Mn^0 over the photon energy range 65 to 270 eV, and thus overlapped the solid-state data. For the solids, only the branching ratios as a function of energy were studied, while for atomic Mn, the 3*s*, 3*p*, and 3*d* angular distributions (beta parameters), absolute partial cross sections, and 3*s* and 3*p* branching ratios were also obtained. However, the details of all but the energy dependence of the branching ratios have been discussed in a separate paper.[27]

EXPERIMENT

The solid-state studies were carried out using both conventional x-ray sources and a tunable synchrotron radiation source provided by the SPEAR storage ring at the Stanford Synchrotron Radiation Laboratory (SSRL). The gas-phase data were collected at the Wisconsin Synchrotron Radiation Center (SRC) using the Aladdin storage ring. The studies using conventional x rays were done in a VG ESCALAB5 spectrometer with nonmonochromatized radiation. Two primary excitation energies were obtained from a twin anode source: Al $K\alpha$ at 1486.7 eV and Mo $M\zeta$ at 192.6 eV. The Al source used the standard anode for the spectrometer. The Mo source was developed for spin-polarized photoelectron-diffraction studies[28] and consisted of a specially designed cap made from 99.97% Mo foil (0.005 in. thick) tightly strapped with *W* wire directly to the Cu surface covering one of the anode faces. In order to provide a high transmissivity of these lower energy x rays, a carbon foil window of 50 $\mu g/cm^2$ separated the source from the sample. The geometry of the chamber fixes the x-ray tube axis at 48° with respect to the axis of the retarding entry lens of a spherical sector analyzer that has been modified to improve its electron optical characteristics and to add a resistive-anode multichannel detector.[29] The sample could be rotated on two axes so as to optimize intensity and to average over photoelectron-diffraction effects in emission from single-crystal samples, using procedures described elsewhere.[28,30]

For all of the experiments done at synchrotron radiation facilities, a Grasshopper monochromator with either a 9001/mm or 6001/mm grating was used to produce monochromatized radiation in the energy range from 65 to 270 eV and with a bandpass of 0.5 Å corresponding to resolutions from $\approx$0.6 eV to $\approx$7 eV, respectively. The upper photon energy limit is attributable to carbon edge absorption from contamination on the optical elements of the monochromators. The radiation polarization at SRC was determined to be 91% in the horizontal plane. At SSRL the angle between the electric field vector and entry axis of the hemispherical sector analyzer of a VG ADES400 was always $\theta=0°$, but at SRC, three energy dispersive analyzers (EDA's) were used concurrently. Each EDA was fixed 90° apart in θ, and mounted on a rotatable disk perpendicular to the direction of the x-ray flux. The rotation axis of this disk was concentric with the radiation incidence direction, thus yielding any θ angle desired between polarization direction and EDA entry. This permitted choosing, for example, the magic angle of $\theta=54.7°$. Since the radiation is linearly polarized, the first and the third EDA's (180° apart) should receive equivalent signals from a gas-phase sample. This apparatus and its operation are described in more detail elsewhere.[26,31]

The surfaces of the solid samples were polished with an oil-based diamond polishing paste down to a particle size 0.5μ. They were then cleaned *in situ* by Ar ion sputtering. A vacuum in the mid 10^{-11} Torr range was maintained throughout the solid-state experiments, except for the SSRL study on MnF_2 where the pressure was a factor of approximately 20 higher. Under these conditions the surfaces were very stable and remained clean for a considerable length of time. Because most of the samples were insulators at room temperature, an electron flood gun (HP 18623A) was used with a current in the 10^2 μA range to suppress possible charging problems.

Since it was also desired in the gas-phase data to obtain accurate absolute binding energies, the well-defined Mn 3*d*, Xe 4*d*, and Ne 2*p* lines were used for calibration. The noble gases were introduced into the source volume simultaneously with the Mn. A binding energy of 14.3 eV was found for Mn 3*d*, in good agreement with Refs. 26 and 32. The internal calibration of the 3*s* and 3*p* manifolds to correct for any nonlinearities in the analyzer system was done in three distinct ways. First, a peak in question was accelerated to the energy position of the 3*d* line, keeping the excitation energy constant and then using the fact that the acceleration potential is the binding energy difference between this peak and the 3*d* peak. Second, and simply the reverse of the first, the 3*d* peak was retarded to the same energy position of the signal of interest. And third, while the acceleration voltage was held constant, the photon energy was increased so as to "superimpose" the desired signal on the 3*d* peak. It was found that these three procedures gave consistent results within our experimental error.

The atomic Mn was produced from high-purity granules heated to approximately 900 °C in a resistively heated Ta oven. The pressure in the source volume was maintained within the mid 10^{-4} Torr range while the chamber was held in the 10^{-9} Torr range. A differentially pumped 12 cm long quartz capillary passed the radiation into the source volume while preventing contamination of the monochromator and the synchrotron storage ring with Mn vapor and other by-products from the heated system. Further details on this gas-phase experimental setup have been discussed in Refs. 26 and 31.

RESULTS AND DISCUSSION

A. Mn 3*s* results

Figure 2 shows solid-state data at two photon energies for $KMnF_3$, and it is obvious that there is a decrease in the ^5S intensity relative to the ^7S when the excitation energy is decreased from 1487 to 193 eV. The two spectra here have had a linear background subtracted from them, but tests of other background subtraction procedures still yield the same clear decrease. The decrease seen here amounts to approximately 28% of the intensity ratio at the high-energy limit.

In order to be sure that such an intensity change for a solid specimen was inherent in the "atomic" photoionization process and not some solid-state effect, we have investigated other possible causes such as crystal structure and surface contaminants. First, for a single crystal, it is well known that strong photoelectron-diffraction effects can occur, and that these depend upon both kinetic energy and direction.[30] In order to rule these out as the source of the variation in branching ratio seen in Fig. 2, two procedures were used: (1) The single crystal $KMnF_3$ sample was studied at both the high and low energies as a function of emission direction, and this should have exposed the full plus/minus effects of diffraction on the branching ratio. The "Δ" in Fig. 2 represents the full excursion of variations seen as a function of direction. They are negligible at the high energy because the kinetic energies are essentially identical. It is thus evident that such effects are at least a factor of 2 less than the overall intensity change observed between the two energies. (2) A polycrystalline MnF_2 sample was used in the same type of experiment to further average out single-crystal effects. The MnF_2 branching ratios were found to be in good agreement with those of the $KMnF_3$ crystal. This is a good test due to the different crystal structures and the different chemical environments encountered by the Mn^{2+} ions in the two crystals. Thus, the two specimens might exhibit different final-state screening contributions to the branching ratio; no such effects were observed. Therefore it seems certain that solid-state effects cannot explain the observed energy dependence.

Since electrons have an energy-dependent mean free path that varies roughly as $\Lambda_e \propto (E_{\rm kin})^{1/2}$, the studies with Mo $M\zeta$ or synchrotron radiation and kinetic energies in the range of 105–111 eV were inherently more surface sensitive than those with Al $K\alpha$ excitation. For the former case, surface structure and contamination effects are thus of more concern. To check for these, Mn 3*s* branching ratios were monitored as a function of takeoff angle, where surface sensitivity is maximized at grazing angles.[30] No significant variations in the branching ratios were observed. We also deliberately altered the surface structure by sputtering without annealing and by exposing the surface to O_2. In both cases the ratio was left unchanged unless severely unrealistic conditions were imposed. Thus, the energy dependence is not a surface effect.

In order to explore further whether this energy dependence of the Mn 3*s* branching ratios is of purely atomic character, Mn gas-phase studies using monochromatic synchrotron radiation at eight energy steps between 113 and 270 eV were performed. Although such a gas-phase study avoids the near-threshold secondary electron background problems which plague corresponding solid-state experiments,[16] a negative aspect of such spectra is that the near-threshold spectral region can be rich in structure and somewhat confused by a number of competing and overlapping effects.[26,33–35] The two lowest photon energies at the bottom of the panel in Fig. 3 illustrate the spectral complexity encountered in this energy region. For the curve with 135 eV photon energy and at a rela-

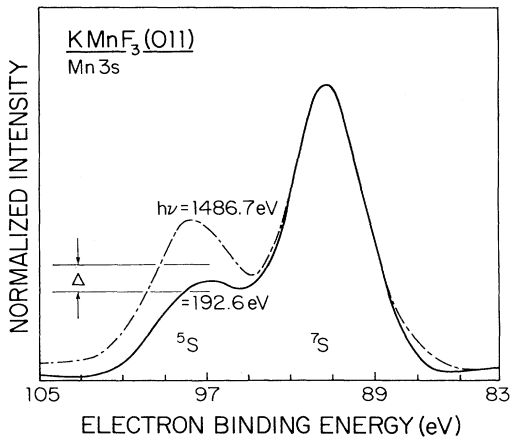

FIG. 2. The Mn 3*s* multiplet from $KMnF_3$(110) obtained with Al $K\alpha$ and Mo $M\zeta$ excitation energies. The quantity Δ represents the upper limit of measured variations in the $^5S(1)$:^7S relative intensity due to angular-dependent diffraction effects for the Mo $M\zeta$-excited 3*s* multiplet. No variation with angle is seen at the higher excitation energy. Δ is thus less than the change due to excitation energy by a factor greater than 2.

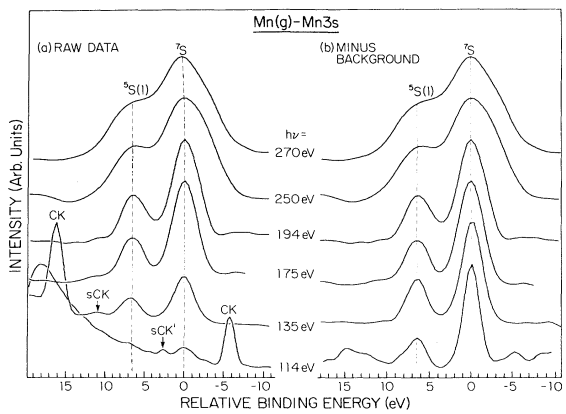

FIG. 3. Raw data and background-corrected data are presented side-by-side for the Mn 3*s* multiplet from gas-phase atomic Mn at various photon energies. The background subtracted from the raw data was the corresponding spectrum from another analyzer for which the polarization direction was perpendicular to the electron detection direction ($\theta = 90°$); it should thus contain only intensity contributions from radiationless decays and secondary electrons.

tive binding energy of approximately 16 eV (or 28 eV kinetic energy), a Coster-Kronig (CK) peak results from the initial photoionization of a $3p(\beta)$ electron (i.e., a $3p$ spin-down electron) with subsequent $4s \rightarrow 3p$ and $3d \rightarrow \epsilon l$ rearrangements.[33,35] Also, at a relative binding energy of approximately 11 eV (or 33 eV kinetic energy), a broader super Coster-Kronig (SCK) peak appears which originates from the emission of a $3p(\alpha)$ electron (i.e., a $3p$ spin-up electron) with subsequent $3d \rightarrow 3p$ and $3d \rightarrow \epsilon l$ rearrangements.[33] Finally, in the 114 eV photon energy curve another small SCK peak appears (denoted as SCK′) at approximately 3 eV relative energy (or 18 eV kinetic energy) which originates from emission of a $3p(\beta)$ electron with subsequent $3d \rightarrow 3p$ and $3d \rightarrow \epsilon l$ rearrangements. This last feature (SCK′) was overlooked in a prior study of Malutzki and Schmidt,[33] possibly due to its coincidental overlap with photoelectron peaks.

From Fig. 3, it is clear that any attempt to extract quantitative information from the near-threshold energy region must include precisely subtracting out the underlying secondary electron background and any peaks due to nonradiative decay. Such a precise subtraction is in fact possible using the three-analyzer data acquisition setup discussed previously. Specifically, all branching ratio data were collected at $\theta = 0°$, thereby yielding a maximum response for s orbital emission into EDA's 1 and 3, and virtually no response for it in EDA 2. However, contributions from radiationless decay processes and the inelastically scattered electron intensity should be distributed in all three EDA's equally. This provides a unique method for removing these artifacts from the desired $3s$-associated spectrum by subtracting the spectrum from EDA 2 from that of EDA 1 or EDA 3. As can be seen in the right panel of Fig. 3, this subtraction process does indeed permit cleaning up the $3s$ doublet to a very high degree. The small broad peaks at left and right in the two bottom curves are probably artifacts of the subtraction procedure, and could be due to the idiosyncrasies of the individual analyzers. Nonetheless this procedure permits deriving Mn $3s$ branching ratios for photon energies down to 113 eV, i.e., only ≈ 15 eV above threshold.

Plotted side-by-side in Fig. 3 are thus the raw data and the background-subtracted data for the photon energies indicated. Three aspects of these data deserve comment. First, there is a degradation of resolution as photon energy is increased. This decrease is indirectly due to the carbon-contaminated optics of the monochromator; the x-ray flux from the Grasshopper monochromator became drastically attenuated in its high-energy region due to carbon K-edge absorption and thus the normal process of increasing the resolution by reducing the bandpass became impractical. Second, the number of usable photon energies used was limited by the need to avoid interference effects between the desired signals and the undesired signals such as Auger, CK, or SCK types of signals. Third, the observation that forms the central theme of this paper is that, as the photon energy used for the $3s$ spectra is decreased to ≈ 114 eV, it is obvious even in the raw data of Fig. 3(a) that the $^5S(1)$ peak has also decreased markedly in intensity relative to ^7S. And the background-substracted spectra of Fig. 3(b) make this trend even more evident. Table II puts these results in more quantitative terms, showing Mn $3s$ branching ratios as a function of electron kinetic energy. The numbers in this table were derived from the background-subtracted spectra using a fitting program with mixed Gaussian-Lorentzian peak shapes. An additional small adjustment was made to each branching ratio to allow for phase-space (final density-of-states) corrections; the intensity ratio was multiplied by the square root of the inverted kinetic energy ratio. Note that at higher energies, since ΔE is only 6 eV, this correction has a small effect. And at lower energies, since the ^5S peak is always at a lower kinetic energy, its corrected relative intensity will go up; thus, the ratios in Table II are if anything conservative

TABLE II. Manganese $3s$ and $3p$ multiplet branching ratios.

	Mn $3s$ data		Mn $3p$ data		
	^7S E_{kin} (eV)	$^5S(1)/^7S$	^7P E_{kin} (eV)	$^5P(1)/^7P$	$^5P(4)/^7P$
Solid state					
MnF_2	1387.4	0.621±0.03	1411.7	0.160±0.03	0.265±0.06
	170.0	0.446±0.05	117.6		0.159±0.04
	93.3	0.410±0.03			
$KMnF_3$	1387.4	0.537±0.04			
	170.0	0.432±0.07			
	93.3	0.420±0.04			
Gas phase					
Mn	170.7	0.448±0.05	100	0.106±0.03	0.153±0.02
	150.7	0.441±0.03	90	0.096±0.03	0.151±0.02
	130.7	0.411±0.03	75	0.096±0.03	0.149±0.02
	94.7	0.444±0.02	60	0.095±0.03	0.121±0.02
	80.7	0.421±0.02	50	0.096±0.02	0.108±0.02
	75.7	0.430±0.02	40	0.091±0.02	0.087±0.02
	35.7	0.447±0.02	25	0.081±0.02	0.055±0.02
	14.7	0.334±0.02	20	0.058±0.02	0.061±0.02

estimates of the observed spectral decreases of ^5S as energy is decreased.

The solid-state data were handled in a similar fashion and since these backgrounds are relatively well behaved at the higher energies utilized, a linear background was used in the fit. These results are also presented in Table II and an overall summary of all of our 3*s* branching ratios is plotted in Fig. 4. (We have reanalyzed the XPS data of Kowalczyk *et al.*[23] for MnF_2 and find a ratio of 0.55 ± 0.04 that is consistent with the average value of 0.58 for MnF_2 and $KMnF_3$ from Table II.) The abscissa is the electron kinetic energy of the higher binding energy multiplet, i.e., the $^5S(1)$ for these 3*s* excitations. The gradual decrease in the $^5S(1)$:^7S branching ratio is evident in the solid-state data over the 100 to 1387 eV range. The gas-phase data at lower energies also overlay the solid-state data well, and show a general downward trend from the high-energy limit that finally drops off very rapidly near threshold. Thus, although it would be very desirable to have atomic data at higher energies approaching the sudden limit so as to better define the precise energy dependence, we feel confident that the highest energy point is a good representation of the XPS limit for Mn^{2+}, and thus also probably for atomic Mn, especially in view of the highly atomic character of the multiplets seen in Fig. 1. The larger error for the higher photon energy spectra resulted from an inherent loss of resolution due to the limitations of the monochromator. At approximately 15 eV above the $^5S(1)$ threshold, the ratio drops significantly, finally going to zero for energies below the $^5S(1)$ threshold. Overall, the solid-state and gas-phase data for emission from Mn^{2+} and Mn^0 thus can be described very well by a single curve, although the precise form of it over the long interval between 200 eV and 1350 eV can only be guessed; the normalized slope of the line assumed is found to be $[dR/dE_{\rm kin}]/R_{\rm SA} = 2.4\times10^{-4}$/eV. The four points for $KMnF_3$ and MnF_2 at lower energies of 93 and 171 eV are fully consistent with a continuation of this smooth curve, with an average normalized slope of 5.4×10^{-4}/eV. The seven points for atomic Mn between 36 and 171 eV yield a lower slope of 5.0×10^{-5}/eV, but are nonetheless consistent within our error limits with the smooth curve shown. An independent analysis of the same atomic Mn data[27] over the 36–151 eV range using a different fitting procedure and weighting points according to their variable error estimates yields a larger normalized slope of 2.3×10^{-4}/eV that is in excellent agreement with the slope from 200 eV to 1350 eV.

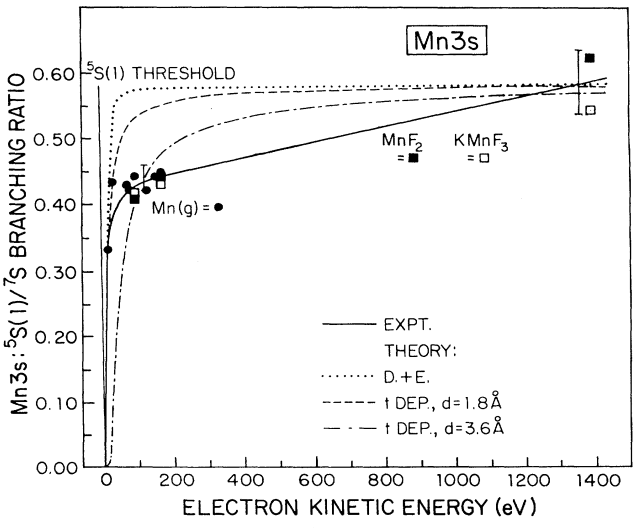

FIG. 4. The energy dependence of the Mn 3*s* branching ratio, $^5S(1)$:^7S, is shown from XPS energies down to approximately 15 eV above threshold. Results for both atomic Mn in the gas phase and the Mn-containing solid compounds $KMnF_3$ and MnF_2 are shown. Also shown are theoretical curves calculated using the direct-plus-exchange model of Eq. (1) (D.+E.) (Ref. 16) and the time-dependent model of Eq. (2) (*t* dep.) (Ref. 17); the parameters used in these calculations are given in the text.

B. Mn 3*p* results

As mentioned above, emission from the Mn 3*p* core level also will exhibit a multiplet structure that can be described by different *L*-*S* term states in a manner analogous to Mn 3*s*. However, the 3*p*, having an $l>0$, will have multiplets that are inherently more complex than the 3*s* due to the added degree of freedom of coupling of orbital angular momentum.[1(a),36] Beyond this, both spin-orbit and crystal-field effects must be considered. This added complexity is illustrated by the overlapping multiplets for both atomic Mn and the compounds MnF_2 and MnO shown in Fig. 5, but here again there is a rather striking similarity of the atomic and solid-state results. Although the more complex origins of these features result in a less accurate theoretical description to date for the origins of the 3*p* manifold,[36,37] the theoretical calculations at the bottom of Fig. 5 nonetheless qualitatively predict the correct form of the spectra, particularly if spin-orbit and crystal-field effects are included as in the work of Yamaguchi, Shibuya, and Sugano[37] (solid curve). These theoretical curves are based on a simple multiplet hole theory (MHT) and do not include any CI effects. The magnitudes of the splittings calculated with the inclusion of spin-orbit and crystal-field effects are smaller than those in experiment; this discrepancy may be due to a slight error in an empirical adjustment of certain Coulomb and exchange integrals in the model. Theory predicts the spectrum to be composed of a single strong ^7P state and several ^5P states at higher binding energies, in qualitative similarity to the case of 3*s* emission. It is also evident from the solid-state data in Fig. 5 that the multiplet features have been broadened relative to those of the gas-phase data. We will focus on the two largest branching ratios derived from such data: the $^5P(1)$:^7P and the $^5P(4)$:^7P. The separation of the $^5P(1)$ from the ^7P of 3.1 eV is considerably less than that of the $^5P(4)$ of 17.7 eV and thus one might expect the former ratio to have an energy dependence more like that of the ^7P state.

An additional complication with 3*p* spectra is that the 3*p* orbital has a radial node and thus its various peaks may exhibit Cooper minima, making their energy dependence more difficult to analyze than the 3*s*. The presence

of the Cooper minima at photon energies of 100–120 eV are clearly evident in the individual absolute cross sections plotted in Fig. 6. From this plot it is clear that the ^7P and the $^5P(1)$ both have a Cooper minimum at the same energy of about 95 eV, although for $^5P(1)$ it is less pronounced. The position of the $^5P(4)$ Cooper minimum is shifted to higher energy by almost exactly the 17.7 eV difference between its kinetic energy and that of the ^7P (cf. Table I).

The behavior very near threshold is, however, difficult to determine precisely due to interference from an underlying SCK transition at the lowest energy used for the $^5P(4)$ of $h\nu=95$ eV. The presence of this same peak can be seen in the 114 eV raw data for 3*s* emission of Fig. 3 at ≈ 3 eV relative energy. Its lack of angular dependence with respect to the polarization vector and its stability relative to the excitation energy suggests an Auger-type decay. Yin *et al.*[38] have performed theoretical calculations for atomic Mn and found the presence of a SCK transition (denoted here as SCK′) in this energy region. Schmidt *et al.*[35] first experimentally confirmed its existence, and in the later work of Malutzki and Schmidt,[33] they evidently overlooked its presence due to an overlap with the $^5P(4)$ peak. Background corrections could be made to the intensity of the $^5P(4)$ signal, however, by subtracting the intensity of the SCK′ peak for the $\theta=90°$ signal at $h\nu=114$ eV. The final intensities were obtained with the same Gaussian-Lorentzian fitting routine used for 3*s*. Table II lists these energy-dependent branching ratios (again with small corrections for the final density of states) as a function of kinetic energy and Fig. 7 plots them. The abscissa of Fig. 7 is electron kinetic energy relative to the $^5P(4)$ or $^5P(1)$ threshold, as appropriate. It should be mentioned that the falloff noted in the $^5P(4)$ intensity begins at about the same energy as its Cooper minimum, which is shifted by approximately 17 eV relative to that of the ^7P peak. This may somewhat exaggerate the drop seen in the $^5P(4)$:^7P branching ratio near threshold. However, the general decrease continues well below the region of the two Cooper minima, and also yields a very smooth curve in this region. The two curves

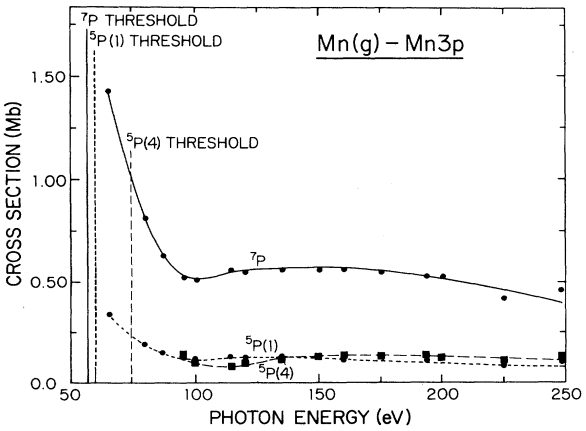

FIG. 6. Individual absolute Mn 3*p* cross sections for atomic Mn are presented for the three strongest multiplet peaks: ^7P, $^5P(1)$, and $^5P(4)$. A weak Cooper minimum is apparent in all three, with a noticeable shift in the $^5P(4)$ position to higher photon energy.

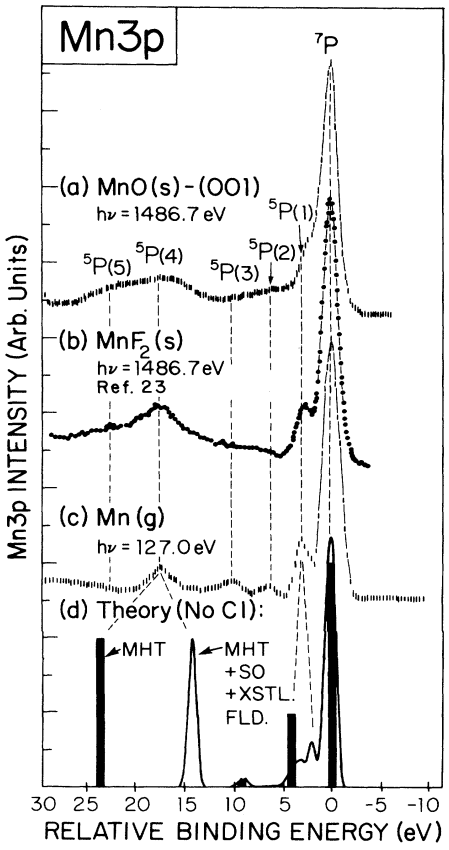

FIG. 5. Experimental Mn 3*p* spectra for (a) MnO(001) (b) polycrystalline MnF_2 (Ref. 36) and (c) gas-phase atomic Mn are compared to one another and in (d) also to the multiplet hole theory calculations of Refs. 36 and 37.

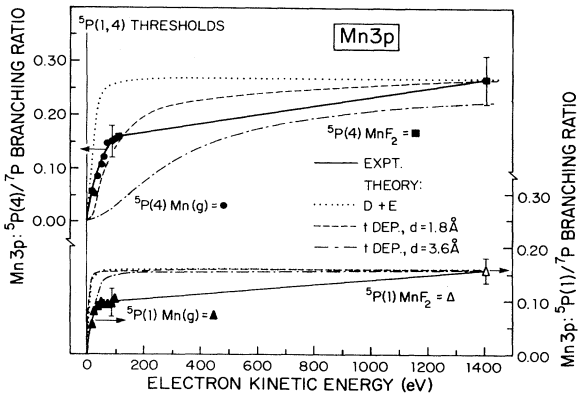

FIG. 7. The energy dependences of the Mn 3*p* branching ratios $^5P(1)$:^7P and $^5P(4)$:^7P are shown over the energy range from the XPS regime down to approximately 20 eV above threshold. Results are shown for both atomic Mn and polycrystalline MnF_2. Theoretical curves using the same models as presented in Fig. 4 are also presented, with relevant parameters given in the text.

in Fig. 7 agree very well with the general shape of that for 3*s* emission in Fig. 4, and for $^5P(4)$ there is again good agreement between solid-state and atomic data. Thus, we conclude that both the 3*s* and 3*p* spectra are influenced by a similar decrease in the intensities of the higher binding energy multiplets as threshold is approached, and that this decrease begins at very high energies of at least 200 eV above threshold. Considering again the normalized effective slopes at higher energies (in this case between 118 and 1412 eV), we find $[dR/dE_{\rm kin}]/R_{\rm SA}=2.6\times10^{-4}$ for $^5P(4)$ and 2.9×10^{-4} for $^5P(1)$, values which are remarkably close to one another and to that for $^5S(1)$ of 2.4×10^{-4}, especially in view of the wide range of energy separations from the septet reference peaks that is involved (17.7 eV, 3.1 eV, and 6.5 eV, respectively). We now discuss some possible theoretical explanations for these similar results for Mn 3*s* and 3*p* branching ratios.

C. Approximate theoretical models

We have previously noted that the two models yielding Eqs. (1) and (2) have been compared with prior shakeup and shakeoff data (as well as energy-dependent data for screening satellites[16]) and have been found to predict some, but not all of the experimental observations. It is thus of interest to explore how well they describe the variation of 3*s* and 3*p* branching ratios in Figs. 4 and 7. Only three values are needed to do this: the sudden-limit value $R_{\rm SA}$ for the branching ratio, which we take to be the XPS values for each of the three ratios considered, the excitation energy ΔE [which is from Table I equal to 6.5 eV for $^5S(1)$, 3.1 eV for $^5P(1)$, and 17.7 eV for $^5P(4)$] and, for use in Eq. (2), the effective distance d traveled by the photoelectron in leaving the system [which we have taken to be either 1.8 Å (the mean radius of the outer 4*s* subshell in Mn, a choice consistent with that of Thomas for neon[17]) or 3.6 Å (twice this distance or the mean 4*s* diameter)]. The larger distance thus represents an approximate upper limit of the time necessary for the photoelectron to leave the atom. Curves calculated with these two equations and these two distances are shown in Figs. 4 and 7, where they are labeled as direct plus exchange (D.+E.) for Eq. (1) and time-dependent (*t* dep.) for Eq. (2). Considering first the 3*s* results in Fig. 4, we see that the agreement with experiment is poor, especially for the behavior at high energy, where only the time-dependent 3.6 Å curve is consistent with the data between approximately 100 eV and the XPS limit; however, the latter curve is not at all consistent with the behavior for energies less than approximately 100 eV. For the 3*p* results of Fig. 7, all three theoretical curves for the $^5P(1)$:^7P ratio with smallest energy separation are in poor agreement with experiment, i.e., theory predicts a sharp rise near threshold and a quick convergence to the sudden limit. It is only for the $^5P(4)$:^7P ratio with the largest ΔE value that a modest degree of agreement is seen for the time-dependent 1.8 Å model; adjusting this distance to slightly below 1.8 Å and/or reducing the effective ΔE should yield better agreement with experiment. However, taking account of the three *P* multiplet ratios considered here shows that neither model well describes our data. [In addition, although both models generally predict a sharp onset of the transition to the sudden limit in the N_2/Ni(110) shakeup or screening satellite experiment,[16] the energy range considered is too limited to yield equivalent results.] It is thus clear from this comparison that better theoretical modeling is required to fully understand the shapes of these 3*s* and 3*p* branching ratios.

A further interesting point in our data is that the overall form of the curves for all three branching ratios studied is very similar, with nearly identical normalized slopes in going from approximately 200 eV to the XPS limit. This is not at all consistent with the ideas embodied in Eqs. (1) and (2), for which the separation of the feature from the main line is a critical parameter in determining the rapidity of approach to the sudden limit. Alternatively, it may suggest that it is the *average* septet-quintet separation as calculated over the entire quintet multiplet that is important, since both the $^5P(1)$ and $^5P(4)$ seem to have the same behavior. This average should be very nearly the same for both the ^5S and ^5P manifolds and should yield a separation from the respective ^7S and ^7P main lines of about 13 eV (the simplest Van Vleck estimate),[1(a),27] and this near equality may be a way to understand this behavior. In fact, these numbers for atomic Mn at $h\nu=127$ eV are found to be 11.9 eV for 3*s* and 9.7 eV for 3*p*. Since it is likely that the ^5P manifold with all of its correlation satellites extends over an energy range of 30 eV or more that is approximately equal to that of the 3*s*, some of the ^5P intensity at largest separations is probably overlapping the 3*s* region (Table I shows that the separation between ^7P and ^7S is only 35.5 eV) and thus not fully included in this average. Thus, the true average separation for 3*p* may be closer to the 11.9 eV of the 3*s* multiplet. However, some rationale for using this average energy in Eq. (2) is needed.

D. More accurate theoretical models

In trying to formulate a more accurate theoretical picture of these phenomena, the example of 3*s* emission already discussed in connection with Fig. 1 suggests that we may need a more complex many-electron approach involving configuration interaction to fully describe the energy dependence of the multiplet manifold. However, to begin with the simplest possible explanation, we consider the state dependence of the one-electron matrix elements leading to the final $^5S(1)$ and ^7S peaks. This has been done by first carrying out HF calculations for the initial state of Mn^{2+} and the fully relaxed ionic final states of Mn^{3+} with a 3*s* hole. Here, the initial-state was the HF function for the $[3s^23p^63d^5]$ ^6S state of Mn^{2+}. For the ionic final states, HF calculations were done for the $[3s^13p^63d^5]$ ^5S and the $[3s^13p^63d^5]$ ^7S configurations of Mn^{3+}. The next step was to calculate the continuum orbitals for each final state in the presence of the Coulomb and exchange interactions of the fully relaxed Mn^{3+} orbitals (one set for ^5S and one for ^7S). This thus yields two separate continuum orbitals, $\epsilon p\uparrow$ for ^5S and $\epsilon' p\downarrow$ for ^7S. The basic matrix elements calculated were then finally $\langle \epsilon p\uparrow|X|3s\uparrow\rangle$ and $\langle \epsilon' p\downarrow|X|3s\downarrow\rangle$, where X is either the

length or velocity form of the dipole operator. This picture thus involves separating out the 3s-to-photoelectron excitation as the "active electron" in the problem (a procedure often used in the sudden approximation), and it also assumes a weak (but nonzero) coupling between photoelectron and ion core. In varying photoelectron energy from low to high values, we can also pass from more sudden to more adiabatic regions of the excitation spectrum.

In discussing such matrix elements and photoelectron spin, it is also important to note that the true N-electron final state must involve the coupling of the ion core to the continuum orbital so as to form the required ^6P final state of the system that results from dipole excitation of ^6S. This coupling via Clebsch-Gordan coefficients results in final overall states of the following form:

$$\Psi_f^1(^6P)=|\phi_f^5(^5S)\epsilon p\uparrow(^2P),^6P\rangle\ , \tag{4}$$

$$\Psi_f^2(^6P)=-(1/7)^{1/2}|\phi_f^7(^7S)\epsilon p\uparrow(^2P),^6P\rangle +(6/7)^{1/2}|\phi_f^7(^7S)\epsilon' p\downarrow(^2P),^6P\rangle\ , \tag{5}$$

where Ψ_f^1 and Ψ_f^2 are the final states for ^5S and ^7S, respectively, $\epsilon p\uparrow$ and $\epsilon p\downarrow$ are the spin-up and spin-down photoelectron, respectively, and certain Clebsch-Gordan coefficients have been given definite values. It is thus clear that the ^5S state involves only the emission of a spin-up electron, while the ^7S involves a mixture of the two, with probabilities of 6/7 for spin down and 1/7 for spin up [yielding nonetheless a very high spin polarization of $(6-1)/(6+1)=71.4\%$ in the ^7S peak]. This will mix the two different one-electron matrix elements for ^7S, and we show in Fig. 8 the appropriate averages over the relevant one-electron matrix elements for the two ionic states involved. These matrix elements were calculated in both length (L) and velocity (V) forms and the agreement between them shown in Fig. 8 is well within the acceptable limits for the HF approximation. Also, it is clear from this figure that any conclusions concerning the energy dependence of the branching ratio made with either the L or V curves will be essentially identical. It is also evident from these two pairs of curves that the difference in the ^5S and ^7S matrix elements is very small (zero to $\approx 5\%$ at maximum) all the way to threshold, and that, even if the small 6.5 eV difference in kinetic energy between ϵ and ϵ' is allowed for, there is still not a sufficient difference to account for the observed changes of more than 25% seen in Fig. 4.

This simple calculation of the threshold effect in a relaxed one-electron approach is clearly not sufficient, and we now discuss a possible basis for the next level of calculations needed. This clearly should involve configuration interaction of the type considered in Fig. 1, but we also wish to include a coupling between the ^5S and ^7S ionic states so that intensity can shift between them. The latter we will refer to as interchannel coupling. This coupling will be most important when the channels involved are nearly degenerate and/or when their relative cross sections change rapidly as a function of excitation energy.

We now consider an example of the overall interactions involved for a Mn 3s manifold that we will label as before by the ionic states ^7S and ^5S. First we use the internal CI configurations given by Bagus, Freeman, and Sasaki[21] to describe the ionic final states with some correlation included:

$$\phi_f^5(^5S)\simeq a_0|3s^1(^2S)3p^6(^1S)3d^5(^6S),^5S\rangle +a_1|3s^2(^1S)3p^4(^1D)3d^6(^5D),^5S\rangle +a_2|3s^2(^2S)3p^4(^3P)3d^5(^3P_1),^5S\rangle +a_3|3s^2(^1S)3p^4(^3P)3d^6(^3P_2),^5S\rangle+\cdots\ , \tag{6}$$

$$\phi_f^7(^7S)\simeq b_0|3s^1(^2S)3p^6(^1S)3d^5(^6S),^7S\rangle +b_1|3s^1(^2S)3p^4(^3P)3d^7(^4P),^7S\rangle+\cdots\ , \tag{7}$$

where the a_i's and b_i's are mixing coefficients and we indicate the overall coupling of spin and orbital angular momenta for each subshell or individual electron, as well as the overall coupling of all electrons. We have here shown only the configurations that Bagus, Freeman, and Sasaki have found to be the most important contributors to these ionic wave functions; they are listed in order of importance in both cases. These functions can now be incorporated into coupled wave functions for the ^5S and ^7S states, respectively:

$$\Psi_f^1(^6P)=C_5^1|\phi_f^5(^5S)\epsilon p(^2P),^6P\rangle +C_7^1|\phi_f^7(^7S)\epsilon' p(^2P),^6P\rangle\ , \tag{8}$$

$$\Psi_f^2(^6P)=C_5^2|\phi_f^5(^5S)\epsilon p(^2P),^6P\rangle +C_7^2|\phi_f^7(^7S)\epsilon' p(^2P),^6P\rangle\ , \tag{9}$$

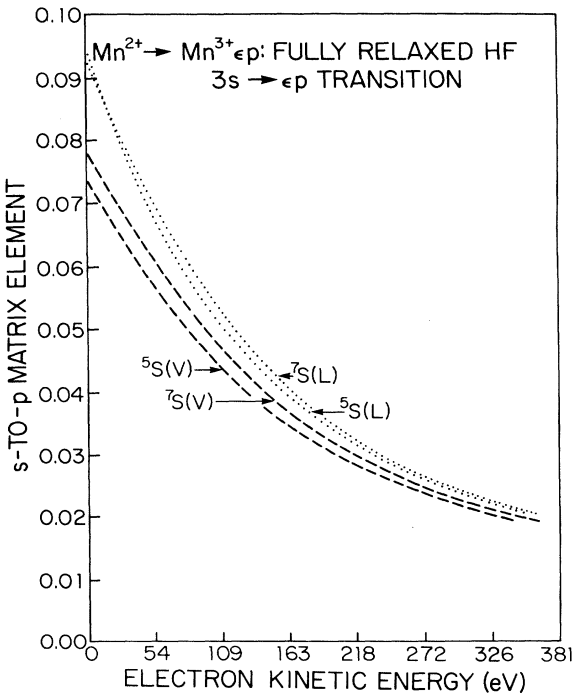

FIG. 8. Hartree-Fock matrix elements for $3s\rightarrow\epsilon p$ excitation in the Coulomb-exchange potentials of fully relaxed Mn^{3+} ionic final states appropriate to the $^5S(1)$ and ^7S multiplet features. These have been evaluated using both the length (L) and velocity (V) forms of the dipole operator. The results are shown as a function of energy above threshold.

where the C_i^j's are mixing coefficients and $|\epsilon' - \epsilon| = \Delta E$, the energy splitting between the two states. We here omit explicit coupling of the various angular momenta to produce the overall ^6P final states required by the dipole transition [cf. Eqs. (4) and (5)], but this is implicitly included. Also, of the several possible states, only the two at lowest energy that would correspond to the $^5S(1)$ and ^7S peaks in the spectra will be discussed. That is, if $C_5^1 = 1$ then all the intensity would be in the ^5S peak and if $C_7^2 = 1$ then all the intensity would be in the ^7S peak; these would be the limits of the normal treatment with no interchannel coupling. Put in terms of the experimental observations, we propose that the energy dependence of the branching ratio results from an energy dependence in the mixing coefficients away from this limit in such a way as to decrease the relative intensity of the ^5S channel in going from high energy to threshold. Whatever the interchannel mixing may be, it must still leave the relevant ionic total energies unchanged, since the final observation of the photoelectron is made after it has left the ion.

We conclude this discussion of theory by mentioning one further aspect of interchannel coupling that could be important. We have described in Eqs. (8) and (9) an interchannel coupling process which only mixes the ^5S and ^7S states. To generalize this further, consideration should also be given to coupling with the $3p$ and $3d$ channels. Although we are concerned with photon energies well above any point of resonance with these channels, interchannel coupling is still possible. Coupling to the $3d$ channel may be more important, since the $3d$ photoionization cross section, as calculated by Yeh and Lindau,[39] shows a substantial increase over the $3s$ and the $3p$ cross sections as the photon energy approaches the $3s$ threshold. The $3p/3s$ cross section ratio is by contrast relatively constant as the $3s$ threshold is approached. This therefore may suggest some degree of $3s$-$3d$ interchannel coupling at lower energies.

We also note some very recent work that bears on the CI+interchannel coupling effects considered here: A theoretical study of $4s$ photoionization from Mn^+ $4s$ (Ref. 40) has also verified the importance of the various forms of correlation discussed above. In addition, a theoretical investigation of $3s$ photoionization from neutral Mn atoms, including in an approximate way some of these correlations,[41] has led to preliminary results which qualitatively agree with our experimental results, thereby further confirming the role played by CI+interchannel coupling.

We conclude on a comparative note by pointing out that these near-threshold results for Mn $3s$ and Mn $3p$ emission are very similar to prior work on shakeup or shakeoff from atoms,[4,8,11] shakeup and screening satellites in molecules,[16,42] and to some degree spin-orbit doublets,[43,44] in their tendency to show a decrease in the relative intensities of the lower-kinetic-energy features as compared to the feature at highest kinetic energy that corresponds to the ground state of the ion. There is clearly a need for a more precise theory of such near-threshold effects and their relationship to the sudden-to-adiabatic transition.

CONCLUSIONS

We have considered the excitation energy dependence of the Mn $3s$ and Mn $3p$ spectral regions in emission from both atomic Mn and several rather ionic Mn compounds (MnF_2, $KMnF_3$, MnO, and $Cd_{0.3}Mn_{0.7}Te$). The energy range is from about 15 eV above threshold to above 1400 eV. The Mn $3s$ multiplet, which should be much less affected by resonance transitions and other final-state complexities than Mn $3p$, $3d$, or $4s$ emission, shows a decrease in the $^5S(1)$:^7S branching ratio as energy is decreased. A significant 28% decrease in this branching ratio is observed over the range from $h\nu = 1487$ to 200 eV, followed by a more abrupt drop at about 15 eV above threshold. Two separate branching ratios in the Mn $3p$ multiplet region [$^5P(1)$:^7P and $^5P(4)$:^7P] have also been studied over the same energy interval, and they are found to exhibit an almost identical form to the $3s$ data in approaching threshold, including again a significant drop over the range $h\nu = 1487$ to 200 eV.

We suggest that these effects are related to the sudden-to-adiabatic transition, but neither of the models applied before to describe the effects of this transition on satellite behavior[16,17] is found to adequately agree with our data. Nor are these effects due simply to changes in the multiplet-specific one-electron matrix elements involved, as we have verified by direct calculation. We have considered qualitatively a more general theoretical model for such effects that includes both CI effects in the final-state ionic wave functions *and* an interchannel coupling between different states of the ion-plus-photoelectron that could act near threshold to shift intensity from the lower-kinetic-energy quintet states of the ion to those associated with the septet ground state of the ion. Finally, we suggest that there may be a common theoretical origin in the near-threshold reductions of the lower-kinetic-energy features in complex core spectra consisting of a main line plus "satellites" of some origin, whether these be due to shakeup, shakeoff, multiplet splittings, spin-orbit splittings, or screening satellites.

ACKNOWLEDGMENTS

This work has been supported by the Office of Naval Research under Contract Nos. N00014-87-K-0512 and N00014-90-J-1457, the National Science Foundation under Grant No. CHE83-20200, the U.S. Dept. of Energy under Contract Nos. DE-AC05-84OR21400 and DE-AC03-76SF00098, and the U.S. Army Research Office under Contract No. DAAL03-86-K-0085. B.H. is grateful for financial support from IBM and C.S.F. benefited from support from the University of Hawaii Foundation, L.U.R.E./University of Paris, Orsay, and C.E.N., C.E.A., Saclay, France. We are indebted to V. Jaccarino and J. K. Furdyna for supplying crystals of MnO and $Cd_{0.3}Mn_{0.7}Te$, respectively. We also gratefully acknowledge the following colleagues for their assistance with obtaining some of the experimental results in this publication: Z. Hussain, J. Lecante, H. Rotermund, M. Sagurton, and J. Stohr.

*Present address: IBM Adstar, San Jose, California 95193.
†Present address: University of California-Davis and Lawrence Berkeley Laboratory.
‡Present address: New York University, New York, New York 10003.
§Present address: Universidad Nacional Autonoma, Mexico, DF, Mexico.
‖Present address: Riber S. A., Paris, France.

[1](a) C. S. Fadley, review in *Electron Spectroscopy: Theory, Techniques, and Applications,* edited by C. R. Brundle and A. D. Baker (Academic, London, 1978), Vol. 2, Chap. 1; (b) G. Wendin, *Structure and Bonding: Breakdown of the One-Electron Pictures in Photoelectron Spectra* (Springer, New York, 1981), Vol. 45.
[2]S. T. Manson, J. Electron Spectrosc. **9**, 21 (1976).
[3]R. L. Martin and D. A. Shirley, J. Chem. Phys. **64**, 3685 (1976).
[4]T. A. Carlson and M. O. Krause, Phys. Rev. **140**, A1057 (1965).
[5]T. Åberg, Phys. Rev. **156**, 35 (1967); T. A. Carlson, C. W. Nester, Jr., T. C. Tucker, and F. B. Malik, *ibid.* **169**, 27 (1968).
[6]D. P. Spears, H. J. Fishbeck, and T. A. Carlson, Phys. Rev. A **9**, 1603 (1974).
[7]P. H. Kobrin, S. Southworth, C. M. Truesdale, D. W. Lindle, U. Becker, and D. A. Shirley, Phys. Rev. A **29**, 194 (1984).
[8]G. B. Armen, T. Åberg, K. R. Karim, J. C. Levin, B. Crasemann, G. S. Brown, M. H. Chen, and G. E. Ice, Phys. Rev. Lett. **54**, 182 (1985).
[9]H. Smid and J. E. Hanson, Phys. Rev. Lett. **52**, 2138 (1984); J. Phys. B **18**, L97 (1985).
[10]K. G. Dyall and F. P. Larkins, J. Phys. B **15**, 219 (1985).
[11]C. E. Brion, K. H. Tan, and G. M. Bancroft, Phys. Rev. Lett. **56**, 584 (1986).
[12]J. Mitroy, K. Amos, and I. Morrison, J. Phys. B **17**, 1659 (1984); J. Mitroy, K. Amos, I. Morrison, I. E. McCarthy, and E. Weigold, *ibid.* **18**, L91 (1985).
[13]M. Y. Adam, F. Wuilleumier, S. Krummacher, V. Schmidt, and W. Mehlhorn, J. Phys. B **11**, L413 (1978).
[14]I. E. McCarthy and E. Weigold, Phys. Rev. A **31**, 169 (1985).
[15]K. T. Leung and C. E. Brion, Chem. Phys. **82**, 87 (1983).
[16]J. Stohr, R. Jaeger, and J. J. Rehr, Phys. Rev. Lett. **51**, 821 (1983).
[17]T. D. Thomas, Phys. Rev. Lett. **52**, 417 (1984); (private communication).
[18]J. W. Gadzuk and M. Sunjic, Phys. Rev. B **12**, 524 (1975).
[19]K. G. Dyall, J. Phys. B **16**, 3137 (1983).
[20]L. Hedman, P. F. Heden, C. Nordling, and K. Siegbahn, Phys. Lett. **29A**, 178 (1969); C. S. Fadley, D. A. Shirley, A. J. Freeman, P. S. Bagus, and J. V. Mallow, Phys. Rev. Lett. **23**, 1397 (1969).
[21]P. S. Bagus, A. J. Freeman, and F. Sasaki, Phys. Rev. Lett. **30**, 850 (1973).
[22](a) B. W. Veal and A. P. Paulikas, Phys. Rev. Lett. **51**, 1995 (1983); B. W. Veal and A. P. Paulikas, Phys. Rev. B **31**, 5399 (1985); (b) S. J. Oh, G. H. Gweon, and J. G. Park, Phys. Rev. Lett. **68**, 2850 (1992).
[23]S. P. Kowalczyk, L. Ley, R. A. Pollak, F. R. McFeely, and D. A. Shirley, Phys. Rev. B **7**, 4009 (1973); S. P. Kowalczyk, Ph.D. thesis, University of California at Berkeley, 1976.
[24]B. Hermsmeier, C. S. Fadley, M. O. Krause, J. Jimenez-Mier, P. Gerard, and S. T. Manson, Phys. Rev. Lett. **61**, 2592 (1988).
[25]R. Bruhn, E. Schmidt, H. Schroeder, and B. Sonntag, Phys. Lett. **90A**, 41 (1982).
[26]M. O. Krause, T. A. Carlson, and A. Fahlman, Phys. Rev. A **30**, 1316 (1984).
[27]J. Jimenez-Mier, M. O. Krause, P. Gerard, B. Hermsmeier, and C. S. Fadley, Phys. Rev. A **40**, 3712 (1989).
[28]B. Sinkovic and C. S. Fadley, Phys. Rev. B **31**, 4665 (1985); B. Sinkovic, D. J. Friedman, and C. S. Fadley, J. Magn. Magn. Mater. **92**, 301 (1991); B. Sinkovic, B. Hermsmeier, and C. S. Fadley, Phys. Rev. Lett. **55**, 1227 (1985); B. Hermsmeier, B. Sinkovic, J. Osterwalder, and C. S. Fadley, J. Vac. Sci. Technol. A **5**, 1082 (1987); B. Hermsmeier, J. Osterwalder, D. J. Friedman, and C. S. Fadley, Phys. Rev. Lett. **62**, 478 (1989); B. D. Hermsmeier, J. Osterwalder, D. J. Friedman, B. Sinkovic, and C. S. Fadley, Phys. Rev. B **42**, 11 895 (1990).
[29]J. Osterwalder, P. J. Orders, M. Sagurton, C. S. Fadley, B. D. Hermsmeier, and D. J. Friedman, J. Electron Spectrosc. Relat. Phenom. **48**, 55 (1989).
[30]C. S. Fadley, Prog. Surf. Sci. **16**, 275 (1984).
[31]M. O. Krause, T. A. Carlson, and P. R. Woodruff, Phys. Rev. A **24**, 1374 (1981).
[32]C. Corliss and J. Suger, J. Phys. Chem. Ref. Data **6**, 1253 (1977).
[33]R. Malutzik and V. Schmidt, *Electronic and Atomic Collisions,* edited by M. J. Coggiola, D. L. Huestis, and R. P. Saxon (North-Holland, New York, 1985), p. 9.
[34]V. Schmidt, Comments At. Mol. Phys. **17**, 1 (1985).
[35]E. Schmidt, H. Schroeder, H. Voss, and H. E. Wetzel, J. Phys. B **17**, 707 (1984).
[36]C. S. Fadley and D. A. Shirley, Phys. Rev. A **2**, 1109 (1970).
[37]T. Yamaguchi, S. Shibuya, and S. Sugano, J. Phys. C **15**, 2625 (1982).
[38]L. T. Yin, J. Adler, T. Tsang, C. H. Chen, D. A. Ringers, and B. Crasemann, Phys. Rev. A **9**, 1070 (1974).
[39]J. J. Yeh and I. Lindau, At. Data Nucl. Data **32**, 1 (1985).
[40]V. K. Dolmatov, J. Phys. B **25**, L629 (1992).
[41]V. K. Dolmatov (unpublished).
[42]A. Reimer, J. Shirmer, J. Feldhaus, A. M. Bradshaw, U. Becker, H. G. Kerkhoff, B. Langer, D. Szostak, R. Wehlitz, and W. Braun, Phys. Rev. Lett. **57**, 1707 (1986).
[43]T. E. H. Walker, J. Berkowitz, J. L. Dehmer, and J. T. Waber, Phys. Rev. Lett. **31**, 678 (1973).
[44]J. Barth, F. Gerken, C. Kunz, V. Radojevic, M. Ildrees, and W. R. Johnson, Phys. Rev. Lett. **55**, 2133 (1985).